2. Lukin V P *Atmosfernaya Adaptivnaya Optika* (Atmospheric Adaptive Optics) (Novosibirsk: Nauka, 1986)
3. Lukin V *Atmospheric Adaptive Optics* (SPIE Press Monograph, PM23) (Bellingham, Wash.: SPIE, 1995)
4. Lukin V P *Opt. Lett.* **4** 15 (1979)
5. Lukin V P, Emaleev O N *Kvantovaya Elektron.* **7** 1270 (1980) [*Sov. J. Quantum Electron.* **10** 727 (1980)]
6. Lukin V P, Matyukhin V F *Kvantovaya Elektron.* **10** 1264 (1983) [*Sov. J. Quantum Electron.* **13** 814 (1983)]
7. Zuev V E, Lukin V P *Appl. Opt.* **26** 139 (1987)
8. Emaleev O N, Lukin V P *Kvantovaya Elektron.* **9** 2264 (1982) [*Sov. J. Quantum Electron.* **12** 1470 (1982)]
9. Lukin V P et al. *J. Opt. Soc. Am. A* **11** 903 (1994)
10. Lukin V P *Proc. SPIE* **2222** 527 (1994)
11. Vitrichenko É A et al. *Problemy Opticheskogo Kontrolya* (Optical Monitoring Problems) (Editor-in-Chief I V Samokhvalov) (Novosibirsk: Nauka, 1990)
12. Vitrichenko É A et al. *Dokl. Akad. Nauk SSSR* **300** 312 (1988) [*Sov. Phys. Dokl.* **33** 309 (1988)]
13. Fortes B V, Lukin V P *Proc. SPIE* **1688** 477 (1992)
14. Lukin V P et al. *Proc. SPIE* **2222** 522 (1994); Lukin V P et al. *Opt. Atmos. Okeana* **8** 409 (1995) [*Atmos. Ocean. Opt.* **8** 210 (1995)]
15. Lukin V P, in *Adaptive Optics. Proc. of a Topical Meeting, Oct. 2–6, 1995, Garching, Germany* (ESO Workshop Proc., No. 54, Ed. M Cullum) (Garching bei München: European Southern Observatory, 1996) p. 373
16. Lukin V P, Fortes B V *Astron. Zh.* **73** 419 (1996) [*Astron. Rep.* **40** 378 (1996)]
17. Lukin V P *Opt. Atmos. Okeana* **9** 1433 (1996) [*Atmos. Ocean. Opt.* **9** 910 (1996)]
18. Lukin V P et al. *Opt. Atmos. Okeana* **12** 1161 (1999) [*Atmos. Ocean. Opt.* **12** 1107 (1999)]
19. Lukin V P *Appl. Opt.-LP* **37** 4634 (1998)
20. Lukin V P *Opt. Atmos. Okeana* **12** 981 (1999) [*Atmos. Ocean. Opt.* **12** 941 (1999)]
21. Lukin V P, Fortes B V *Adaptivnoe Formirovanie Puchkov i Izobrazheniĭ v Atmosfere* (Adaptive Beaming and Imaging in the Atmosphere) (Novosibirsk: Izd. SO RAN, 1999)
22. Lukin V P, Fortes B V *Adaptive Beaming and Imaging in the Turbulent Atmosphere* (SPIE Press Monograph, PM109) (Bellingham, Wash.: SPIE, 2002)
23. Kanev F Yu, Lukin V P *Opt. Atmos.* **4** 1273 (1991) [*Atmos. Opt.* **4** 878 (1991)]
24. Lukin V P, Fortes B V *Appl. Opt.-LP* **41** 5616 (2002)

PACS numbers: 07.07.Dr, 42.30.Wb
DOI: 10.1070/PU2003v046n08ABEH001654

Adaptive distributed optoelectronic information-measuring systems

Yu N Kul'chin

1. Introduction

The process of intensive development and promotion of optical fiber telecommunication systems has led to the emergence of one of the most rapidly developing fields of optoelectronics — fiber optical sensors (FOSs) of physical quantities [1]. The organic combination of a communication system and the system of monitoring of physical quantities in a common path of the optical fiber (OF) opens up considerable opportunities for the development of lengthy and ramified information-measuring systems (IMSs) whose functional destination and configuration can be continuously improved without recourse to additional communication lines. In this case, an important advantage of the FOSs is that they introduce into the IMSs such properties as high sensitivity, low dimensions, immunity to electromagnetic interference and environmental attack, the possibility of multiplexing individual sensors into complex measuring systems, and potentially low cost [2]. The above-enumerated virtues and the change-over from discrete FOSs of physical quantities to extended distributed FOSs, which have begun to show in recent years, have made it possible to commence the development of distributed fiber measuring networks (DFMNs) and 'sensitive surfaces' capable of reconstructing the spatial parameter distributions of the physical fields (PFs) under investigation [3].

The transfer to higher-dimension DFMNs, the development and improvement of the processing methods of data arrays at the DFMN output, involving the use of new physical phenomena and the application of modern neural network technologies of signal processing, open up broad opportunities for endowing IMSs with such new properties as the ability to learn and adapt [4, 5]. This is an important step on the road to the production of practical distributed IMSs intended for the investigation of PFs and the monitoring of the state of technical and technological objects.

The aim of our report is to consider the approaches to the solution of the development problem of adaptive distributed optoelectronic IMSs as one of the promising lines of modern physical instrument making.

2. Tomographic DFMNs for reconstructing the distributions of scalar and vector physical fields

The traditional approach to the reconstruction problem of multidimensional physical-field distribution functions through the use of DFMNs consisting of a set of 'point' FOSs, wherein measurements correlate with a definite discrete set of points in space, does not always meet with success owing to the technical difficulties arising in the multiplexing/demultiplexing of the signals received from a large number of 'point' FOSs. This does not permit us to attain a high spatial resolution and a fast response [1, 3]. Unifying 'point' FOSs sequentially in an extended optical fiber measuring line (OFML) or employing distributed FOSs makes it possible to obtain an integral phase or amplitude signal of the action of an external PF on the FOSs along the OF laying path [3, 6].

In the general case, the integral signal of PF action on the OFML can be represented as [7–16]

$$g(p,\phi) = \int_{L(p,\phi)} h(x,y,\phi)\,\mathrm{d}L\,, \tag{2.1}$$

where $h(x,y,\phi)$ is the function of OFML responsivity to the PF action:

$$h(x,y,\phi) = \begin{cases} qf(x,y) \text{ for a scalar PF}\,, \\ q\hat{F}\big[\mathbf{A}(x,y),\mathbf{m}(x,y,\phi)\big] \text{ for a vector PF}\,, \end{cases}$$

where $f(x,y)$ is the spatial distribution function for the PF parameter being recorded, $\mathbf{A}(x,y)$ is the intensity vector of the field under investigation, $\mathbf{m}$ is the unit vector of the tangent ($\mathbf{e}$) or normal ($\mathbf{n}$) to the OFML laying contour, $\hat{F}[\,..\,]$ is an operator, x,y are the Cartesian coordinates in the detection plane (S), q is a constant coefficient which defines the responsivity per unit OFML length to the PF parameter to be measured, L is the coordinate along the OFML laying contour, and (p,ϕ) are the polar coordinates defining the OFML contour position in the detection plane (see Fig. 1a).

The signals described by expression (2.1) bear the indirect information on the PF parameters distribution function.

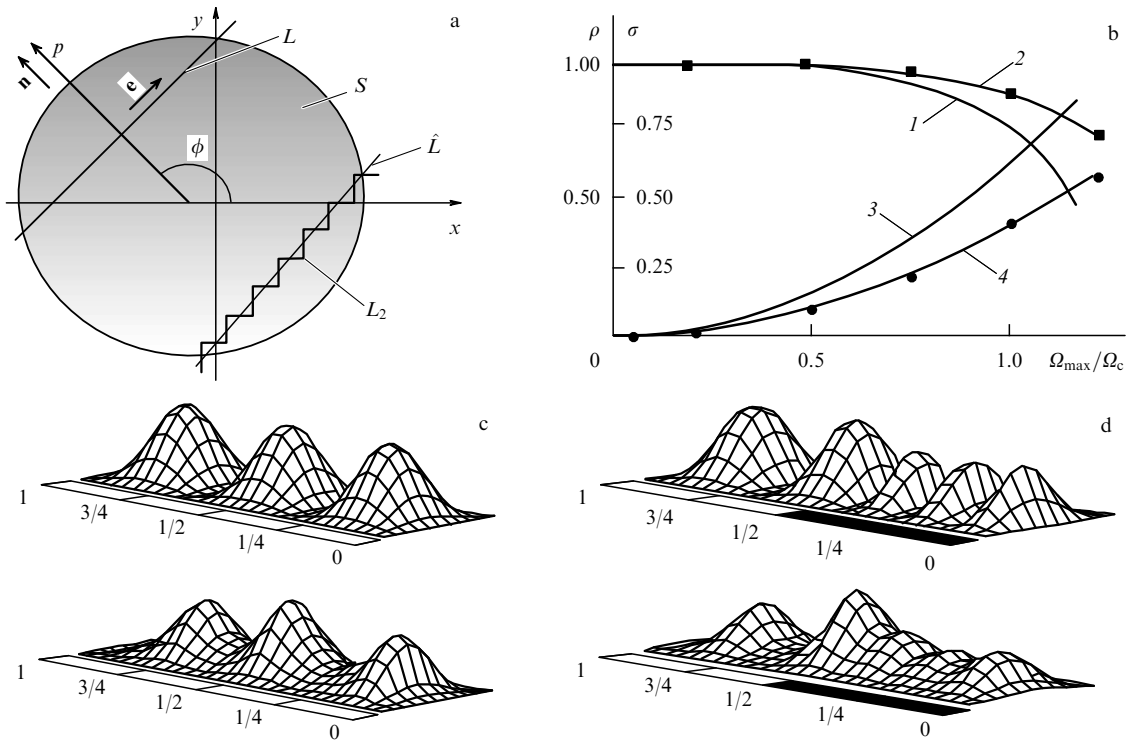

Figure 1. Reconstruction of physical field distributions with the use of a DFMN: (a) OFML arrangement in the domain of PF realization; (b) calculated (*1*, *3*) and experimental (*2*, *4*) dependences of the correlation coefficient ρ (*1*, *2*) and the root-mean-square error σ (*3*, *4*) for the initial and reconstructed PF distribution functions, and (c, d) calculated (top) and experimental (bottom) intensity distributions of transverse wall vibrations of empty and half-filled metal vessels, respectively.

Special-purpose mathematical techniques are therefore required for its reconstruction. For a scalar PF, such methods are based on the tomography theory [17]. According to this theory, to solve the problem of $f(x, y)$-function reconstruction requires obtaining a set of integral images $g(p, \phi)$ for different polar coordinates (p, ϕ). This set of images will constitute a direct Radon transform of the sought-for $f(x, y)$ function; its reconstruction necessitates applying the procedure of inverse Radon transform to the data set obtained [17, 18].

For a vector PF, the problem of reconstructing the parameters distribution $\mathbf{A}(x, y)$ has no direct solution by tomographic techniques. That is why for each kind of $h(x, y, \phi)$ dependence one has to apply a measurement data processing technique on its own.

The existing algorithms of computerized tomography permit a rather exact reconstruction of original scalar PF functions only when the sampling frequency in each of the parameters p and ϕ of the Radon transform (2.1) is high enough. In our case, the requisite sampling can be obtained by covering the plane S with a distributed fiber measuring network composed of OFMLs laid at certain intervals along the radial and angular coordinates [7 – 10]. One of the virtues of this approach lies in the possibility of obtaining the real-time scanning results. The requisite periodicity of readings in the polar angle and the polar radius in the DFMN is defined by the following expressions [17]

$$\Delta\phi = \frac{\pi}{D\Omega_{\max}}\,, \qquad \Delta p = \frac{\pi}{\Omega_{\max}}\,, \tag{2.2}$$

where D is the characteristic transverse dimension of the domain S, and $\Omega_{\max}$ is the maximum spatial frequency of physical field variations.

Since the construction of an OFML-network-based IMS involves a limitation of the number of integral readings (2.1), this leads to incorrectness of the solution of the inverse problem of PF reconstruction [9, 10]. Therefore, for the most trustworthy reconstruction of the original from an incomplete set of integral data, the computational reconstruction algorithm should be supplemented with the rule for evaluating the originals of functions to be reconstructed with the aid of dependences having the minimal norm of departure from its average value in the S domain [8, 10]. And the DFMN itself should meet the requirement that its characteristic spatial frequency determined from the expression $\Omega_{\mathrm{c}} = \sqrt{6K/S}$ (where K is the number of OFMLs appearing in the network) be greater than the frequency $\Omega_{\max}$ [8, 10]. The combined action of the above requirements is illustrated by the calculated and experimental dependences of PF reconstruction quality parameters on the Ω_{c}-to-$\Omega_{\max}$ frequency ratio (see Fig. 1b) [9].

To illustrate the use of a DFMN for reconstructing scalar PF distributions, Figs 1c and 1d show experimental and calculated findings obtained in the reconstruction of the intensity distribution of transverse wall vibrations of metal reservoirs for different filling levels of liquid [8, 9].

When the action of a vector PF on the output OFML signal is proportional to the projection of $\mathbf{A}(x, y)$ onto the direction of the unit vector $\mathbf{e}$ tangent to the OFML axis, expression (2.1) can be represented as [13, 16]

$$g(p, \phi) = \int_{(L)} \mathbf{A}(L)\mathbf{e}\,\mathrm{d}L = C(p, \phi)\sin\phi - B(p, \phi)\cos\phi\,, \tag{2.3}$$

where

$$C(p,\phi) = \int_{(L)} A_X(x,y)\,\mathrm{d}L\,, \quad B(p,\phi) = \int_{(L)} A_Y(x,y)\,\mathrm{d}L$$

are the coefficients which carry information on the Radon transform of the projections of the field intensity $\mathbf{A}(x,y)$ onto the Cartesian axes X and Y, respectively. To separate the contributions from the quantities C and B to the total integral signal it is expedient to take advantage of a combined DFMN with additional OFMLs laid similarly to the initial ones, but sensitive to the projection of the field intensity vector $\mathbf{A}(x,y)$ onto the vector of the normal ($\mathbf{n}$) to the OFML axis. The integral signal at the output of these additional OFMLs can be described by the expression

$$g_1(p,\phi) = \int_{(L)} \mathbf{A}(L)\mathbf{n}\,\mathrm{d}L = C(p,\phi)\cos\phi + B(p,\phi)\sin\phi\,. \tag{2.4}$$

The combined solution of Eqns (2.3) and (2.4) gives $C = g\sin\phi + g_1\cos\phi$ and $B = -g\cos\phi + g_1\sin\phi$. (We note that the contributions of the quantities C and B are also separated when employing an additional curvilinear OFML unevenly responsive across the length [13, 16].) In this way the reconstruction problem for the distribution of the Cartesian components of the intensity of a vector PF reduces to the above-considered tomographic problem of reconstruction of a scalar quantity distribution function from the known integral images.

According to Eqns (2.3) and (2.4), employing OFMLs of only one type in a DFMN, for instance, those sensitive to the vector projection onto the OF axis, makes it possible to reconstruct only the eddy constituent of the vector PF [14–16]. And employing a DFMN on the base of the OFMLs sensitive to only the vector projection onto the normal to the OF axis permits the reconstruction of only the potential component of the vector PF [14–16]. The operating capacity of such DFMNs was experimentally borne out by the example of reconstruction of an electrostatic field distribution in Ref. [12].

In each specific case of investigation of a vector PF, the choice of ML laying trajectory in a DFMN depends on the type of OFMLs being used. For instance, in the problems on the reconstruction of longitudinal displacement field distributions advantage should be taken of the OFMLs wherein the action of the vector field on the OF is proportional to the fiber-tangential derivative of the longitudinal component of the vector $\mathbf{A}$: $\partial A_L/\partial L$. (Such OFMLs can be made, for instance, on the base of extended fiber interferometers [14–16].) In this case, it is expedient to lay the OFMLs in a polygonal trajectory composed of similar rectangular steps (L_2 in Fig. 1a). For these OFMLs, the magnitude of the integral signal (2.1) is defined by the expression

$$g(p,\phi) = \int_{(L_2)} \mathrm{d}L_2 \left(\frac{\partial(\mathbf{A}\cdot\mathbf{e})}{\partial L_2}\right) = \sqrt{2}\int_{(\hat{L})} \left(\frac{\partial A_x}{\partial x} + \frac{\partial A_y}{\partial y}\right)\mathrm{d}\hat{L}$$
$$= \sqrt{2}\int_{(\hat{L})} \operatorname{div}\mathbf{A}(x,y)\,\mathrm{d}\hat{L}\,. \tag{2.5}$$

A new path of integration $\hat{L}$ was introduced in expression (2.5) — a straight line oriented along the stepwise contour (Fig. 1a). It is evident that expression (2.5) constitutes an element of the Radon transform of the function $\operatorname{div}\mathbf{A}(x,y)$ for given values of the polar coordinates (p,ϕ). Hence, by employing a DFMN consisting of stepwise OFMLs it is possible to solve the problem of tomographic reconstruction of the $\operatorname{div}\mathbf{A}(x,y)$ distribution, i.e., to reconstruct the potential component of the vector field.

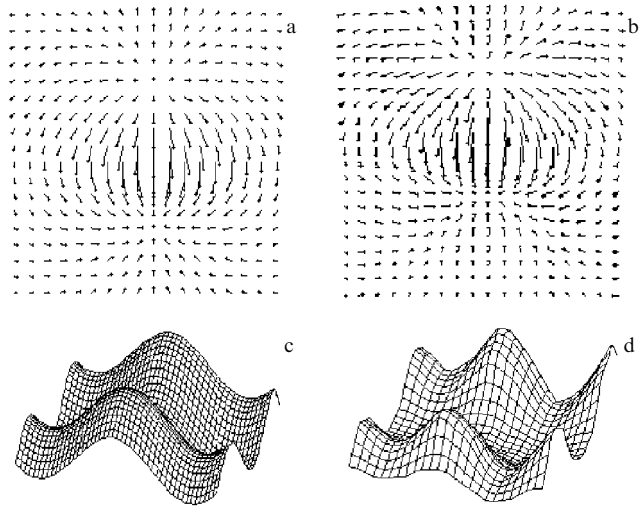

Figure 2. Tomographic reconstruction of the parameter distributions of vector PFs using a DFMN: (a) calculated distribution of the potential component of the longitudinal deformation field of a plane object; (b) distribution of the potential component of the longitudinal deformation field of a plane object, reconstructed from DFMN signals; (c) calculated distribution of the modulus squared of the gradient vector of an elastic-plate transverse displacement field, and (d) distribution of the modulus squared of the gradient of an elastic-plate transverse displacement field, reconstructed from DFMN signals.

At the same time, reconstructing the distribution of the eddy constituent of a vector PF requires using stepwise OFMLs whose signal is formed under the action of the derivative of the PF-vector transverse component in the direction of the tangent to the OF: $\partial A_n/\partial L$. In this case, the execution of the inverse Radon transformation will result in the reconstruction of $\mathbf{k}\cdot\operatorname{rot}\mathbf{A}(x,y)$-function distribution which describes the eddy nature of the PF [14, 15]; here $\mathbf{k}$ is the normal to the plane (x,y).

In the study of longitudinal deformations of elastic surfaces in Refs [14–16], a DFMN made of stepwise interferometric OFMLs was rigidly attached to the surface under investigation. Figure 2a displays the lines of the displacement field being studied, and Fig. 2b shows the result of its reconstruction from the signals of the measuring network (the correlation coefficient between the distributions given is equal to 0.95).

The action of a vector PF on an OFML can also be proportional to the square of the projection of the $\mathbf{A}(x,y)$-vector longitudinal component onto the direction tangential to the OF: $(A_L)^2$. A problem of this type arises, for instance, when the gradient of the transverse displacement field of elastic surfaces acts on an interference-type OFML [13–16]. When the OFML is laid along the L_2 trajectory (see Fig. 1a), the signal obtained at its output takes the form

$$g(p,\phi) = 0.5\int_{(L_2)} \left(\mathbf{A}(x,y)\cdot\mathbf{e}\right)^2 \mathrm{d}L_2 = \int_{(\hat{L})} \left|\mathbf{A}(x,y)\right|^2 \mathrm{d}\hat{L}\,. \tag{2.6}$$

In this way by performing the inverse Radon transform for the data array obtained by a DFMN, it is possible to

reconstruct the distribution function of the PF intensity vector modulus squared. This conclusion was experimentally verified in Refs [13 – 16]. The calculated and experimentally reconstructed distributions of the modulus squared of the gradient vector of a thin-elastic-plate transverse deformation are shown for comparison in Figs 2c and 2d.

3. Extended OFMLs on the base of single-strand multimode interferometers and methods of adaptive spatial filtering

The development of DFMNs for tomographic IMSs designed for monitoring the PF parameter distributions involves the solution of one of the key problems: the production of extended OFMLs. Such OFMLs can be made on the base of practically any distributed or quasi-distributed physical-quantity FOSs whose description and classification are given elsewhere [3]. At the same time, the studies reported in Refs [7 – 9, 13 – 16] showed that FOSs made on the base of single-fiber multimode interferometers (SMIs) are best suited for the production of OFMLs in tomographic fiber measuring networks (FMNs). In an SMI, to measure the magnitude of PF action advantage is taken of the result of intermodal interference of the modes guided through a common multimode OF. SMI-based OFMLs possess a high responsivity, are capable of guiding high-power radiation, and do not necessitate the employment of a reference arm, which advantageously distinguishes them from other types of interferometric measuring devices.

The radiation at the SMI output is a complex (speckled) optical signal which results from the interference of a large number of guided modes with different phase velocities. The action on the SMI is responsible for additional phase shifts between the OF modes, manifesting itself in the correlated spatial restructuring of the speckled pattern [19]. This allowed us to propose the correlation methods of spatial filtering for the processing of the radiation from the SMI. These methods involve the use of amplitude and holographic spatial filters, the signal power at their output being represented as [20 – 22]

$$P_{\text{out}}(t) = \iint_S I(x,y,t)\,T\big(I_0(x,y,0)\big)\,\mathrm{d}x\,\mathrm{d}y\,, \tag{3.1}$$

where $I_0(x,y,0)$ and $I(x,y,t)$ are the radiation intensity distributions in the plane of the spatial filter at the stages of filter recording and processing the SMI signals, respectively, $T(I_0(x,y,0))$ is the transmission function of the spatial filter, S is the filter area, and t is the time.

The investigation of mode phase modulation in multimode OFs and the correlation processing of the radiation from SMIs revealed that the correlation signal power for both types of spatial filters is the function of maximal additional phase difference $\Delta\Phi_{\max}(t)$ between the guided modes in the SMI [21, 22]:

$$P_{\text{out}}(t) \propto \sin c^2\left(\frac{\Delta\Phi_{\max}(t)}{2}\right). \tag{3.2}$$

That is why the metrological characteristics of SMI-based OFMLs are defined by the numerical aperture, the length, and the material of the OFs in use. As a consequence, the SMI sensitivity threshold with respect, for instance, to the relative OF deformation may vary in the range from 10^{-10} to 10^{-5}, and the dynamic range of measurements in the static mode may amount to 30 – 40 dB [3].

Like for all types of optical fiber interferometers, the problem of low-frequency interference signal fading caused by random uncontrollable actions like temperature drift, technological vibrations, random mechanical actions, the drift of laser frequency, etc. is topical for SMI-based OFMLs [3]. To produce practical FMN systems intended for long-term PF monitoring, original adaptive techniques of processing and stabilizing the operational characteristics of extended OFMLs were therefore developed, which relied on the methods of adaptive spatial filtering (ASF) of the radiation field from the SMIs [23 – 25, 37].

An efficient approach to the realization of the ASF method involves the employment of the effects of nonlinear optical interaction of the light waves in photorefractive crystals (PRCs), for instance, in $Bi_{12}TiO_{20}$. Exposing these crystals to radiation with a nonuniform intensity distribution produces a spatially nonuniform distribution of electric charge inside of them. This is responsible for changes in the refractive index of the PRC material, which are proportional to radiation intensity gradients [26 – 28]. Its consequence is the enhancement of the effects of self-diffraction of a light wave (the fanning effect) [28 – 30] and the polarization self-modulation of radiation [31, 32].

When the radiation from the SMI enters the PRC, it is scattered by the inhomogeneities of the crystal. The fields of interference of the scattered waves with the principal wave produce chaotically oriented volume dynamic diffraction gratings in the PRC. Selecting specific crystal dimensions and orientation, the angle of radiation input to the PRC, and the state of radiation polarization, amplification of the scattered waves occurs at these dynamic diffraction gratings (the fanning effect). The efficiency of principal wave conversion to the fanning waves may be as high as 90% [33]. The spatial – angular selectivity of such a set of dynamic gratings (for a crystal length of 10 mm) may be as strong as $\sim 10^{-4}$ rad, making them extremely sensitive to variations of intensity distribution in the field of radiation from the SMI.

As shown in Ref. [23], the fanning wave produced by the SMI radiation at the PRC output is the correlation signal whose power is proportional to the correlation function of the distributions of the field complex amplitudes for the output SMI radiation prior to $[U_1(x,y,0)]$ and after $[U_2(x,y,t)]$ the PF action on the SMI:

$$P_{\text{out}}(t) \propto \operatorname{Re} \iint_S U_2^*(x,y,t)\,U_1(x,y,0)\,\mathrm{d}x\,\mathrm{d}y\,. \tag{3.3}$$

This furnished a way of producing efficient spatial filters for the realization of the ASF method, when processing the SMI signals. The scattered-wave competition observed in the PRC leads to the production of a stationary set of volume dynamic diffraction gratings with a correlation-filter recording time constant τ_R. That is why any fast variations ($\tau < \tau_R$) of the SMI radiation field at the PRC input will have no effect on the state of the spatial filter, which will result in the modulation of the output signal $P_{\text{out}}(t)$ in accordance with expression (3.3). When the variations are slow ($\tau > \tau_R$) or infrequent, the old correlation field will be deleted and a new one will be produced to correspond to the modified radiation intensity distribution at the PRC input. In this case, the output signal $P_{\text{out}}(t)$ would remain unchanged.

The results of experimental investigations into the ASF method of SMI signals processing [23, 24] outlined above have demonstrated not only its high efficiency, but also the long-term stability of its operational characteristics (more

than 8 h), as well as the possibility of processing signals with frequencies above 0.1 MHz.

The effect of polarization self-modulation consists in the variation of the state of polarization of the radiation (with a nonuniform intensity distribution) propagating through the PRC, which is a consequence of radiation-induced time-dependent nonuniform distribution of the refractive index in the crystal [26, 31, 32]. The occurrence of anisotropy of PRC optical properties manifests itself in that the radiation transmitted through the crystal varies in intensity at the output of an analyzer placed behind it [34, 35]. The transmission function of the 'PRC – analyzer' pair can be represented as [26]

$$T_{\mathrm{PSM}}(x,y) = \cos^2\left(a\left[E_{\mathrm{A}} + E_{\mathrm{SC}}(x,y)\right]\right), \tag{3.4}$$

where a is a constant which takes into account the crystal and radiation properties, E_{A} is the intensity of the external electric field, and $E_{\mathrm{SC}}(x,y)$ is the intensity of the internal electric field, which depends on the SMI-radiation field intensity gradient in the PRC.

The series of investigations carried out in Ref. [25] revealed that the 'polarizer – PRC – analyzer' combination placed at the SMI output is capable of fulfilling the function of an amplitude spatial filter in accordance with expression (3.1) and ensuring its ability to adapt for uncontrollable actions, thereby realizing the method of ASF-processing of SMI signals.

In Ref. [36], an investigation was made into the mutual influence of the radiation fields from different SMIs, which overlap in the PRC volume. The optical field overlapping was found to lower the intensity of correlation signals and to have no effect on their information constituent, which opens the door to the development of multichannel systems for signal processing by the ASF method.

In paper [37], an investigation was reported of the feasibility of realizing the ASF method on the basis of an analog electronic device which consisted of a photodiode array spatially matched with the speckled pattern of the SMI radiation field and a multichannel electric-signal processing unit efficient in the processing of signals of an OFML built around OFs of few modes.

4. Neural network techniques of signal processing in distributed optical fiber IMSs

The development of DFMN-based IMSs of large dimensions or a high resolving power is inextricably entwined with the solution of several problems: the real-time processing of large information flows; the recognition and classification of reconstructed PF patterns; the adaptation of the measuring system to the operating conditions and the specific problem, etc. This was the motivation for employing neural network computational methods of tomographic data processing in distributed IMSs, which implies the most radical solution to the above problems [3, 38 – 44]. As shown in Refs [38, 45], it is expedient to employ in the distributed IMSs the perceptron-type multilayer neural networks (NNs) owing to the convenient DFMN-matching interface and the feasibility of a purely optoelectronic realization.

To accomplish the tomographic PF parameter distribution reconstruction from the data array obtained from the DFMN, the perceptron should perform the following functional transformation

$$\mathbf{Y} = F(\mathbf{X}), \tag{4.1}$$

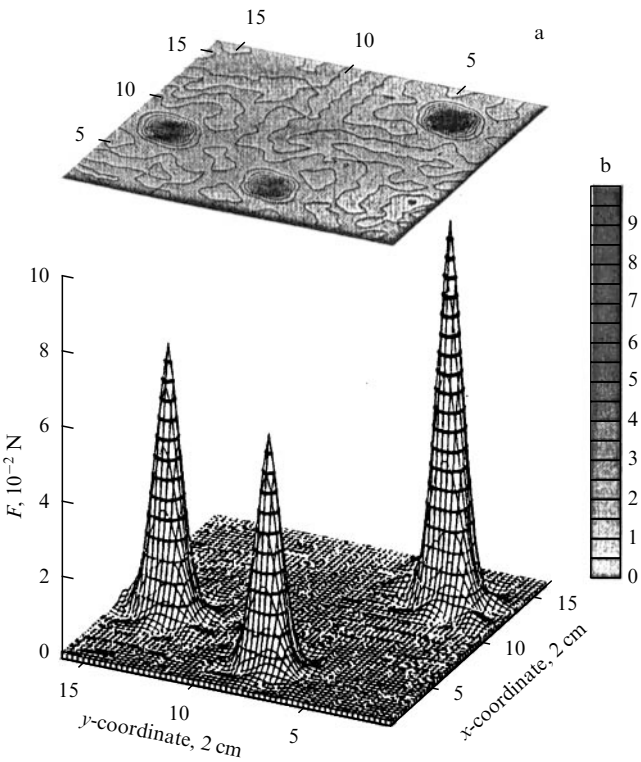

Figure 3. Experimentally reconstructed spatial distribution of the action of gravity on a DFMN, obtained with the use of an optoelectronic NN: (a) contour diagram of the isolevels of a gravitational field, and (b) spatial distribution of gravity.

where $F(\ldots)$ is the functional of the inverse Radon transform, $\mathbf{X} = (x_1, x_2, \ldots, x_N)$ is the input neural-network data vector composed of the magnitudes of the signals at the output of every OFMN in the DFMN, and $\mathbf{Y} = (y_1, y_2, \ldots, y_M)$ is the output data vector composed of the array of reconstructed PF parameter values.

The functional $F(\ldots)$ in expression (4.1) is defined by the matrices of the coupling coefficients between the neurons of input, output, and internal NN layers [45, 46]. For instance, the components of the output vector for a three-layer NN are defined as

$$y_i = \sum_j \omega_{ij} s_j = \sum_j \omega_{ij} f\left(\sum_l w_{jl} x_l\right), \tag{4.2}$$

where ω_{ij} and w_{jl} are the corresponding coupling matrix coefficients between the NN layers, $i = (1, \ldots, N)$, $j = (1, \ldots, M)$, N is the number of OFMLs in the DFMN (the number of input neurons), M is the number of PF reconstruction points (the number of output neurons), l is the number of neurons in the intermediate layer, which depends on the requisite reconstruction quality of PF parameter values, and $f(\ldots)$ is the transfer function.

The reconstruction accuracy of the PF distribution is determined by the quality of NN learning, i.e., the choice of the values of coupling matrix elements and the form of transfer functions [46]. To learn, use is made of a learning page which consists of input and output vector pairs $(\mathbf{X}, \mathbf{Y}')^{\mu}$, where μ is the pair number. During learning they endeavor to minimize the quadratic error mismatch between the requisite and reconstructed PF distributions given in the learning page [38 – 44].

The results obtained in Ref. [42] demonstrated that employing NNs makes it possible to extend the capabilities of distributed IMSs because of using the entire transfer OFML characteristic, and not just its linear portion. This is achieved through the optimal combination of the conjugate-gradient, gradient descent, and thermal annealing methods in the course of perceptron learning [42–44] and the use of the transfer function of the form $f(\ldots) = \tanh(\ldots)$.

The elaborated notions of NN structure and learning methods were realized in Refs [41, 43] in the development of an optoelectronic NN with a holographic coupling matrix, which enables a real-time reconstruction of the PF parameter distribution in the IMS with an accuracy of 6 to 20%, whose operation is illustrated in Fig. 3.

5. Conclusions

The aim of this report was to outline the results that have led to advances in a new area of physical instrument making, which emerged at the interface between several modern fields of knowledge, namely, laser physics, optoelectronics, and artificial intelligence. The emergence of this area is associated with an impetuous introduction into practice of processes and objects which should be monitored and controlled in real time. These problems bring to the fore the necessity to develop high-precision, high-reliable, and fast-response measuring devices with a capacity to adapt to specific conditions of their operating, learning, and solving problems when the data obtained are deficient, and which also have the capacity for pattern recognition and situation prediction. In the future, the problems of development of the physical principles and production technologies of adaptive optoelectronic IMSs should therefore become central to their practical application.

References

1. Kersey A D *Opt. Fiber Technol.* **2** 291 (1996)
2. Butusov M M et al. *Volokonnaya Optika i Priborostroenie* (Fiber Optics and Instrument Making) (Ed. M M Butusov) (Leningrad: Mashinostroenie, 1987)
3. Kul'chin Yu N *Raspredelennye Volokonno-Opticheskie Izmeritel'nye Sistemy* (Distributed Optical Fiber Measuring Systems) (Moscow: Fizmatlit, 2001)
4. Pinchevskiĭ A D *Izmerit. Tekh.* (8) 3 (1991) [*Meas. Tech.* **34** 741 (1991)]
5. Ivanov V N, Kavalerov G I *Izmerit. Tekh.* (10) 8 (1991) [*Meas. Tech.* **34** 978 (1991)]
6. Malekhanov A I *Izv. Vyssh. Uchebn. Zaved. Radiofiz.* **31** 1388 (1988)
7. Kul'chin Yu N et al. *Kvantovaya Elektron.* **20** 513 (1993) [*Quantum Electron.* **23** 444 (1993)]
8. Kul'chin Yu N, Vitrik O B *Izmerit. Tekh.* (3) 24 (1999)
9. Kul'chin Yu N et al. *Izmerit. Tekh.* (3) 32 (1995) [*Meas. Tech.* **38** 304 (1995)]
10. Vitrik O B et al., in *Distributed and Multiplexed Fiber Optic Sensor IV* (Proc. SPIE, Vol. 2294, Eds A D Kersey, J P Dakin) (San Diego: SPIE, 1994) p. 165
11. Kotov O I et al. *Pis'ma Zh. Tekh. Fiz.* **16** (2) 90 (1990) [*Sov. Tech. Phys. Lett.* **16** 81 (1990)]
12. Ginevskiĭ S P et al. *Kvantovaya Elektron.* **22** 1013 (1995) [*Quantum Electron.* **25** 978 (1995)]
13. Kul'chin Yu N et al. *Kvantovaya Elektron.* **22** 1009 (1995) [*Quantum Electron.* **25** 974 (1995)]
14. Kul'chin Yu N et al. *Kvantovaya Elektron.* **24** 467 (1997) [*Quantum Electron.* **27** 455 (1997)]
15. Kulchin Yu N et al. *Fiber Integrated Opt.* **17** 75 (1998)
16. Kul'chin Yu N et al. *Izmerit. Tekh.* (6) 21 (1999) [*Meas. Tech.* **42** 541 (1999)]
17. Natterer F *The Mathematics of Computerized Tomography* (Stuttgart: B.G. Teubner, 1986) [Translated into Russian (Moscow: Mir, 1990)]
18. Tikhonov A N, Arsenin V Ya *Metody Resheniya Nekorrektnykh Zadach* (Solutions of Ill-Posed Problems) 2nd ed. (Moscow: Nauka, 1979) [Translated into English (New York: Halsted Press, 1977)]
19. Bykovskiĭ Yu A et al. *Kvantovaya Elektron.* **17** 1080 (1990) [*Sov. J. Quantum Electron.* **20** 996 (1990)]
20. Kul'chin Yu N, Obukh V F *Kvantovaya Elektron.* **13** 650 (1986) [*Sov. J. Quantum Electron.* **16** 424 (1986)]
21. Bykovskiĭ Yu A, Vitrik O B, Kul'chin Yu N *Kvantovaya Elektron.* **17** 1377 (1990) [*Sov. J. Quantum Electron.* **20** 1288 (1990)]
22. Bykovskiĭ Yu A et al. *Kvantovaya Elektron.* **17** 95 (1990) [*Sov. J. Quantum Electron.* **20** 83 (1990)]
23. Kamshilin A A, Jaaskelainen T, Kulchin Yu N *Appl. Phys. Lett.* **73** 705 (1998)
24. Kulchin Yu N et al., in *Distributed Fiber Optical Sensors and Measuring Networks* (Proc. SPIE, Vol. 4357, Ed. Yu N Kulchin) (Bellingham, Wash.: SPIE, 2001) p. 130
25. Kulchin Yu N, Romashko R V, Kamenev O T, in *Fundamental Problems of Optoelectronics and Microelectronics* (Proc. SPIE, Vol. 5129, Eds Yu N Kulchin, O B Vitrik) (Bellingham, Wash.: SPIE, 2003) p. 168
26. Kamshilin A A et al. *Appl. Phys. B: Laser Opt.* **68** 1031 (1999)
27. Borodin M V et al. *Izv. Vyssh. Uchebn. Zaved. Fiz.* **44** (10) 38 (2001) [*Russ. Phys. J.* **44** 1050 (2001)]
28. Feinberg J *J. Opt. Soc. Am.* **72** 46 (1982)
29. Voronov V V et al. *Kvantovaya Elektron.* **7** 2313 (1980) [*Sov. J. Quantum Electron.* **10** 1346 (1980)]
30. Xie P et al. *J. Appl. Phys.* **74** 813 (1993)
31. Kamshilin A A et al. *Opt. Lett.* **24** 832 (1999)
32. Kamshilin A A et al. *Appl. Phys. Lett.* **74** 2575 (1999)
33. Cronin-Golomb M, Yariv A *J. Appl. Phys.* **57** 4906 (1985)
34. Arizmendi L, Cabrera J M, Agullo-Lopez F *Int. J. Optoelectron.* **7** 149 (1992)
35. Kobozev O et al. *J. Opt. A: Pure Appl. Opt.* **3** L9 (2001)
36. Kul'chin Yu N et al. *Pis'ma Zh. Tekh. Fiz.* **26** (12) 23 (2000) [*Tech. Phys. Lett.* **26** 505 (2000)]
37. Kulchin Yu N et al. *Opt. Eng.* **36** 1494 (1997)
38. Kul'chin Yu N, Kamenev O T, in *Kibernetika i Vuz* (Cybernetics and Institute of Higher Education) Issue 28 (Tomsk: TPU, 1994) p. 3
39. Kulchin Yu N et al. *Opt. Memory Neural Networks* **6** 149 (1997)
40. Kulchin Yu N, Kamenev O T *Laser Biology* **4** 625 (1995)
41. Kul'chin Yu N, Denisov I V, Kamenev O T *Pis'ma Zh. Tekh. Fiz.* **25** (6) 65 (1999) [*Tech. Phys. Lett.* **25** 235 (1999)]
42. Kulchin Yu N, Panov A V *Pacific Sci. Rev.* **3** 1 (2001)
43. Kulchin Yu N et al., in *Fundamental Problems of Optoelectronics and Microelectronics* (Proc. SPIE, Vol. 5129, Eds Yu N Kulchin, O B Vitrik) (Bellingham, Wash.: SPIE, 2003) p. 162
44. Kulchin Yu N et al., in *Fundamental Problems of Optoelectronics and Microelectronics* (Proc. SPIE, Vol. 5129, Eds Yu N Kulchin, O B Vitrik) (Bellingham, Wash.: SPIE, 2003) p. 176
45. Mikaelian A L et al. *Opt. Memory Neural Networks* **1** 7 (1992)
46. Wasserman Ph D *Neural Computing: Theory and Practice* (New York: Van Nostrand Reinhold, 1989) [Translated into Russian (Moscow: Mir, 1992)]

PACS numbers: **42.62.–b**, 87.56.By, 87.59.Dj
DOI: 10.1070/PU2003v046n08ABEH001655

Laser electron-beam X-ray source for medical applications

E G Bessonov, A V Vinogradov, M V Gorbunkov, A G Tur'yanskiĭ, R M Feshchenko, Yu V Shabalin

1. Introduction

At present, a rich variety of diagnostic procedures and interventions in cardiology, neurosurgery, etc. are performed with X-ray monitoring. In so doing, X-ray tubes remain the